

The Air-Launched Autonomous Micro Observer

STEVEN R. JAYNE,^a W. BRECHNER OWENS,^a PELLE E. ROBBINS,^a ALEXANDER K. EKHOLM,^a NEIL M. BOGUE,^b AND ELIZABETH R. SANABIA^c

^a *Physical Oceanography Department, Woods Hole Oceanographic Institution, Woods Hole, Massachusetts*

^b *MRV Systems, San Diego, California*

^c *Oceanography Department, U.S. Naval Academy, Annapolis, Maryland*

(Manuscript received 13 April 2021, in final form 28 December 2021)

ABSTRACT: The Air-Launched Autonomous Micro Observer (ALAMO) is a versatile profiling float that can be launched from an aircraft to make temperature and salinity observations of the upper ocean for over a year with high temporal sampling. Similar in dimensions and weight to an airborne expendable bathythermograph (AXBT), but with the same capability as Argo profiling floats, ALAMOs can be deployed from an A-sized (sonobuoy) launch tube, the stern ramp of a cargo plane, or the door of a small aircraft. Unlike an AXBT, however, the ALAMO float directly measures pressure, can incorporate additional sensors, and is capable of performing hundreds of ocean profiles compared to the single temperature profile provided by an AXBT. Upon deployment, the float parachutes to the ocean, releases the air-deployment package, and immediately begins profiling. Ocean profile data along with position and engineering information are transmitted via the Iridium satellite network, automatically processed, and then distributed by the Global Telecommunications System for use by the operational forecasting community. The ALAMO profiling mission can be modified using the two-way Iridium communications to change the profiling frequency and depth. Example observations are included to demonstrate the ALAMO's utility.


KEYWORDS: Ocean; Hurricanes; Ocean dynamics; Mixed layer; Aircraft observations; Instrumentation/sensors

1. Introduction

We describe the technical development and initial applications of a small ocean profiling float, the Air-Launched Autonomous Micro Observer (ALAMO). The ALAMO can be deployed by an aircraft to make observations of the ocean structure upstream, during the passage, and in the wake of tropical cyclones. It offers the opportunity to provide persistent monitoring of the upper ocean covering a time span of many months to over a year. Designed to have the same size and form factor as an airborne expendable bathythermograph (AXBT), but with the same capabilities as profiling floats used in the Argo program, it provides several hundreds of profiles compared with the single profile measured by an AXBT.

Hurricane forecast accuracy remains a challenging scientific problem (Gall et al. 2013). While hurricane track forecast skill has significantly improved over the past several decades, advancements in intensity forecasts have only begun to show slow, yet steady, improvement since the early 2000s (Walker et al. 2006; DeMaria et al. 2007; Rappaport et al. 2009, 2012; DeMaria et al. 2014; Kimberlain and Brennan 2017; Cangialosi et al. 2020; Gopalakrishnan et al. 2020). The track of a tropical cyclone¹ is

¹ In this paper we use the terms hurricane and tropical cyclone interchangeably.

 Denotes content that is immediately available upon publication as open access.

Corresponding author: S. R. Jayne, surje@alum.mit.edu

determined by the propagation of the storm through the structure of atmospheric winds. Since the ocean is the primary energy source for tropical cyclones (Byers 1944; Palmén 1948; Riehl 1950; Malkus and Riehl 1960; Emanuel 2004), the storm's intensity is sensitive to the heat content and stratification of the upper ocean along the track (Marks et al. 1998; Emanuel et al. 2004; DeMaria et al. 2005; Yablonsky and Ginis 2009; Lin et al. 2013a; Halliwell et al. 2015; Mogensen et al. 2017). Reducing this uncertainty is critical to improving hurricane intensity forecast accuracy, particularly during periods of rapid intensification, which require a warm and deep ocean surface layer (Bosart et al. 2000; Shay et al. 2000; Kaplan and DeMaria 2003; Hendricks et al. 2010). Conversely, cold ocean surface temperatures and/or very shallow mixed layers overlaying cold layers have been shown to significantly weaken even strong hurricanes before landfall (Seroka et al. 2016; Kossin 2017; Miles et al. 2017). Tropical cyclone intensity forecast accuracy also depends on storm-induced mixing and air–sea exchange processes. Uncertainties in the parameterizations of these processes contribute to errors in intensity forecasts (Price 2009; Balaguru et al. 2018).

It had been generally considered a rule of thumb that sea surface temperatures (SST) greater than 26°C were necessary for tropical cyclone formation (Byers 1944; Palmén 1948; Fisher 1958), and the tropical cyclone had to remain over warm water to continue to grow and maintain strength [though see Cione (2015) for a more nuanced discussion of this precondition]. Satellite observations of SST can be a useful predictor of tropical cyclone intensity (DeMaria and Kaplan 1994). However, other metrics of the upper-ocean temperature structure such as hurricane (tropical cyclone) heat potential (Leipper and Volgenau 1972; Gray 1979; DeMaria et al. 2005), the average of the expected mixing

depth of the ocean (Price 2009; Lin et al. 2013b), or the average of the mixed layer temperature are more closely related to the intensity of tropical cyclones than SST (Wada and Usui 2007; Knaff et al. 2013). These integral measures quantify the upper-ocean thermal energy that is accessible by a tropical cyclone. However, they require subsurface information that is not readily available from satellites. Proxy estimates of the ocean's internal thermal structure can be made from satellite altimetry, with the sea surface height anomalies correlated to upper-ocean heat content variability using climatological data (e.g., Carnes et al. 1990; Shay et al. 2000; Goni and Trinanés 2003; Shay and Brewster 2010; Meyers et al. 2014) or more complex methods of estimation [Pun et al. 2016; see Goni et al. (2009) for a discussion]; however, all of these methodologies require in situ data for correlation and validation.

Coupled atmosphere–ocean tropical cyclone forecast models show improved forecast skill relative to uncoupled atmospheric models (Doyle et al. 2014; Ito et al. 2015; Alaka et al. 2020). In particular, the intensity forecast can be improved by coupling to an interactive ocean model. Mogensen et al. (2017) found that in the European Centre for Medium-Range Weather Forecasts (ECMWF) model, the largest forecast sensitivity for intensity was over areas of low ocean heat content. In regions of high heat content (warm, deep mixed layers), tropical cyclones can tap into a nearly unlimited supply of enthalpy, which leads to intensification. However, in regions of marginal tropical cyclone potential, the cyclone intensity is limited by the ocean's thermal energy and the feedback between the cyclone and ocean becomes important. Therefore, they concluded that a realistic ocean model was also required to predict cyclone intensity. Halliwell et al. (2008, 2011) showed that coupled models need to assimilate ocean data to have a correct initial state. It has been demonstrated that increasing the number and frequency of ocean observations will improve both forecast model initialization and the understanding of ocean–atmosphere interactions (Baranowski et al. 2014; Chen et al. 2017a).

The paucity of in situ temperature observations is the limiting factor in monitoring and understanding the interaction of a tropical cyclone and the ocean (Emanuel et al. 2004). The vast majority of the real-time in situ observations of the ocean temperature and salinity structure come from the Argo profiling array (Roemmich et al. 2009; Legler et al. 2015; Riser et al. 2016). However, its nominal spatial spacing of one float per $3^\circ \times 3^\circ$ and temporal sampling of every 10 days is sparse in both time and space, and not well suited for studying tropical cyclones. A few studies have estimated the ocean impact on tropical cyclones by chance encounters with Argo floats (i.e., Lin et al. 2009; Park et al. 2011; Cheng et al. 2015; Johnston et al. 2021), but these observations are infrequent and cannot target a particular tropical cyclone at a given time. Sanabia et al. (2013) elucidated the impact of real-time upper-ocean temperature profile observations from AXBTs in improving both tropical cyclone track and intensity forecasts.

The temperature structure of the upper ocean changes rapidly during its interaction with a tropical cyclone (Chang and Anthes 1978; Price 1981; Gill 1982; Cione and Uhlhorn 2003; Sanford et al. 2007; Knaff et al. 2013). Tropical cyclones drive both mixing and upwelling in the ocean below them, mixing

warm surface water with deeper, colder water. This well-known phenomenon creates a “cold wake” behind the storm, which is stronger on the righthand side of the cyclone (in the Northern Hemisphere) due to inertial currents inducing shear-driven mixing at the base of the mixed layer (Leipper 1967; Stramma et al. 1986; Nelson 1998; D'Asaro et al. 2007, 2014). The cold wake can also weaken the tropical cyclone's intensity since the colder water will decrease the enthalpy flux into the storm (Balaguru et al. 2015; Chen et al. 2017b). Also, cold wakes from previous hurricanes can influence subsequent storms (Brand 1971; Balaguru et al. 2014; Karnauskas et al. 2021). Therefore, real-time rapidly repeating measurements of the quickly changing ocean thermal structure in the vicinity of the tropical cyclone are essential for accurate intensity forecasting.

As part of the Coupled Boundary Layers Air–Sea Transfer (CBLAST) experiment (see Black et al. 2007; Sanford et al. 2007, 2011) during Hurricane Frances (2004) and the Impact of Typhoons on the Ocean in the Pacific (ITOP) experiment (see D'Asaro et al. 2011; Mrvaljevic et al. 2013) during Typhoon Fanapi (2010), upper-ocean data were collected from air-deployed floats. These large (in the range of 30–50 kg in weight and 200–400 dm³ in dimension) profiling floats were deployed from the open ramp door of a U.S. Air Force Reserve Command (AFRC) WC-130J during flights far ahead of tropical cyclones. This procedure is not possible during operational weather reconnaissance missions given the weather conditions. It is, however, possible to utilize the “sonobuoy” launch tube installed on the AFRC WC-130J or NOAA WP-3D Hurricane Hunter planes during routine tropical cyclone reconnaissance missions (i.e., that is used for AXBT launches; see Sanabia et al. 2013) to deploy oceanographic instrumentation.

The significant economic impact of the damage from tropical cyclones, in particular “Superstorm” Sandy (2012) on the eastern seaboard of the United States, spurred efforts to improve the forecasting of hurricanes and nor'easters (or bomb cyclones; Sanders and Gyakum 1980). With NOAA Sandy Supplemental funding the ALAMO float was developed to meet the objective of deploying persistent ocean profilers during operational missions. These upper-ocean observations would be used both to measure the ocean heat content ahead of the hurricane and to understand the evolution of the ocean response during and after the storm. This development was based on a conceptual design of an air-deployed profiling float funded under prior Office of Naval Research funding to Scripps Institution of Oceanography. ALAMO float technical characteristics and capabilities are described in section 2. Example observations are highlighted in section 3, and section 4 offers insight into current and potential future use.

2. ALAMO characteristics

The ALAMO float works on the same basic principles as the Autonomous Lagrangian Circulation Explorer (ALACE) profiling float originally designed by Davis et al. (1992), which was later developed into the Sounding Oceanographic Lagrangian Observer (SOLO; Davis et al. 2001), and thence the SOLO-II profiling floats used in the Argo program today [Roemmich et al.

2019; see Gould (2005) for a review of the development of float technology]. Indeed, the ALAMO represents a natural engineering progression from those original float designs utilizing a redesigned, more efficient buoyancy engine, and smaller, modern electronic controllers. The ALAMO float profiles vertically in a similar manner as its predecessors. To ascend, a pump moves oil from an internal bladder to an external bladder increasing the volume of the float, which increases the float buoyancy. To descend, a valve is opened allowing the oil to flow into the internal bladder, decreasing buoyancy. SOLO-I and APEX floats have an external air bladder to more efficiently increase their volume at the sea surface (Davis et al. 2001). These bladders occasionally failed due to fish bite and exposure to large pressure differences. The ALAMO float uses a dual-chambered internal bladder. At depth, oil is pumped from the oil-filled part of the reservoir. At the surface the valve connecting the bladder to the oil pump is closed and the second part of the bladder is filled with air, which further displaces oil from the first chamber into the external reservoir. This system has a similar improved efficiency at the surface as the SOLO-I, but eliminates the failure modes of an external air bladder (Dufour and Newville 2017). To descend from the sea surface, the air chamber is deflated, oil flows into the internal bladder due to the internal ALAMO vacuum pressure and the external bladder is emptied.

The ALAMO was designed to meet the size and weight requirements for an “A-size” sonobuoy, which is specified by MIL-S-81478C as 123.82 mm (4.875 in.) in diameter, an overall length of 914.39 mm (36 in.), and a weight of no greater than 9 kg for the entire package, including the air-deployment rigging and parachute. As a result, the ALAMO pressure case is thinner than its predecessors and has a maximum operating pressure of 1200 dbar. The displacement volume is roughly 9 L and its weight in air is approximately 9 kg after ballasting. When the external bladder is inflated, the change in volume of the float is 390 mL, yielding a ratio of volume change to total volume, $\Delta V/V$, of 4.2%, compared with 3.4% for SOLO-II floats, and ~1% for APEX floats (Riser et al. 2018). This higher ratio provides ample buoyancy to profile the upper ocean and also raise the antenna sufficiently out of the water even in the high sea state under a tropical cyclone. This added buoyancy also allows the float to profile over larger density differences between the maximum profile depth and the sea surface, which can be helpful in regions such as the Arctic Ocean where a seasonal fresh surface layer creates a strong density barrier.

Advancements in electronics have reduced the size and improved the power efficiency of float controller boards. The ALAMO utilizes a low-power Advanced RISC Machine (ARM) controller with a real-time clock. With a real-time clock driving the system interrupts, the float can be tasked to perform events at specified times, i.e., to perform a profile daily at 1200 UTC.

The ALAMO float acquires data from its global positioning system (GPS) receiver at the beginning and end of each surface period. The floats utilize the commercial Iridium satellite system, which provides global, low-latency, two-way data communications to return their data (IOOC 2004). The data from the conductivity–temperature–depth (CTD) sensors, GPS location information, and engineering data are compressed and

transmitted back to shore using a two-way Iridium transceiver as Short Burst Data (SBD) messages with a maximum length of 340 bytes. The total number of SBD messages for a dive cycle will depend on the number of data points in the profile. While it is possible to return data at as high a vertical resolution as the sensors sample, to reduce Iridium transmission times and associated costs, data are usually averaged to 1-dbar bins for transmission. For a typical profile this results in about 10 SBD messages which are transmitted while the float is at the surface for around 15 min. As with Argo program data (Roemmich et al. 2009), the ALAMO hurricane project hydrographic data can be distributed in real time via the Global Telecommunication System (GTS) for use by forecasting centers.

The float can be reprogrammed during its mission to change the frequency and maximum depth of its profiling, as well as the depth resolution of the data binning. Parameters specifying the float’s behavior can be modified using the two-way Iridium system; SBD messages containing new parameter settings, for example, to reprogram the profiling frequency and depth, vertical speed, drift or parking depth, and sensor sampling characteristics, can be queued in the Iridium system and downloaded when the float surfaces and completes its data uplink (examples of typical missions are shown in Fig. 3). Typical profiling modes are rapid upper-ocean profiling achieving 13 profiles a day of the upper 300 m (Fig. 3a), profiling four times a day from parking at a drift depth of 300 m (Fig. 3b), and profiling once per day from 1000 m while parking at a drift depth of 500 m between profiles (Fig. 3c).

Spring-loaded, foldable fins near the bottom of the float act to stabilize the float at the ocean’s surface in the same manner as the damping disk on other profiling floats (Davis et al. 1992). The fins are folded up and held in place with water-soluble tape before the deployment. The tape dissolves in seawater once the floats are deployed in the ocean, allowing the fins to spring out. The fins feather down when the float is moving upward, but resist downward motion thus damping out oscillatory vertical motion when the float is in the surface wave field ensuring improved stability for satellite communications (Dufour and Newville 2018). Field tests demonstrated that the ALAMO float can rise at a maximum rate of $>45 \text{ cm s}^{-1}$ and descend at a rate of 25 cm s^{-1} . The stability fins feather down when the float is moving rapidly upward causing the difference in speeds. The ascent rate is determined by the amount of oil in the external bladder, and the floats are generally programmed to profile at approximately 10 cm s^{-1} , similar to the ascent speed of an Argo float (Johnson et al. 2007).

The initial ALAMO floats utilized the RBR*duo* temperature and pressure sensors mounted on the top cap (Fig. 1). The RBR*duo* is a commercially available sensor, with an accuracy of $\pm 0.002^\circ\text{C}$ for temperature, and $\pm 0.1\%$ of the full scale pressure (2000 dbar), equating to 2 dbar accuracy in pressure (as calibrated by the manufacturer). Direct measurement of pressure removes the bias errors in the depth estimate induced by uncertainty in the fall-rate equation of the XBTs (e.g., Heinmiller et al. 1983; Roemmich and Cornuelle 1987; for a discussion, see Cheng et al. 2016). The sensors sample at 1 Hz and the raw data are averaged into depth bins, with 1 dbar usually being adequate to resolve the upper-ocean structure; however,

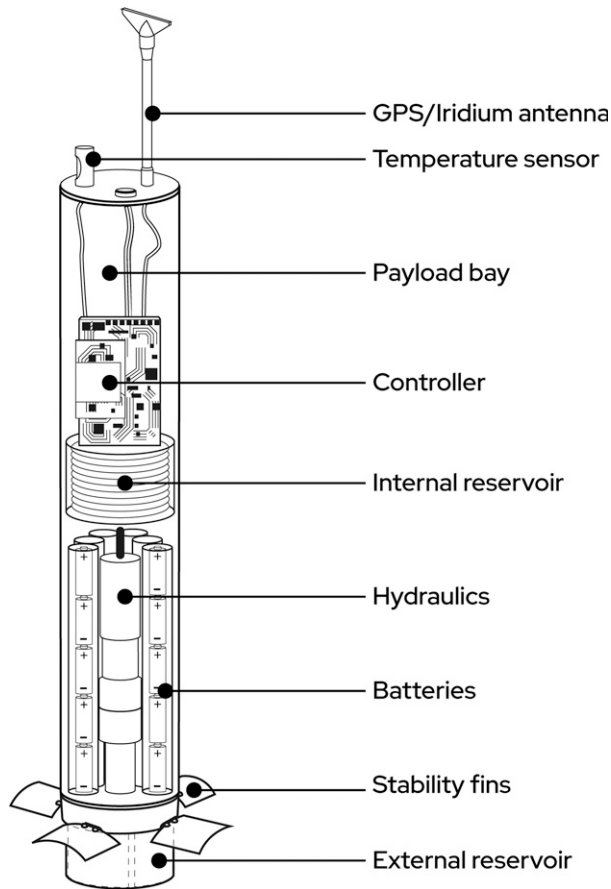


FIG. 1. Schematic of the ALAMO float: The ALAMO float is composed of an anodized aluminum tube, with the temperature and pressure sensors along with a combined GPS and Iridium antenna mounted on the top cap. Inside the float there is a payload bay that contains the electronics for the sensors and the controller. A dual-chambered internal bladder contains oil in one chamber and air in the other. A hydraulic pumping system moves oil from the internal reservoir to the external reservoir on the bottom end of the float. Batteries power the controller, the sensor suite, and the hydraulic pump. Stability fins mounted on the outside of the float near the bottom dampen heaving oscillations when the float is at the ocean surface.

this is a parameter that can be configured depending on the application. Later models have been equipped with the RBRargo³, an inductive CTD designed for Argo floats to measure conductivity from which, in combination with temperature, salinity can be derived. The conductivity sensor has a quoted accuracy of $\pm 0.003 \text{ mS cm}^{-1}$, or approximately $\pm 0.003 \text{ PSU}$ [more details about the sensor can be found in Halverson et al. (2020)]. It is noted that because of the extra space needed on the top cap for the conductivity cell, ALAMOs with a CTD do not currently adhere to the “A-size” requirement, as they are slightly longer than the specification ($\sim 1 \text{ m}$).

As with most autonomous oceanographic instruments, the lifetime of the floats is limited by battery capacity. The largest

fraction of electrical energy is consumed by the pressure work of the hydraulic system pushing oil into the external bladder at depth. The lithium batteries have a total capacity of 36 A h; the floats are able to perform a cumulative vertical profile distance of over 200 000 dbar before battery depletion. The most industrious float to date (serial number 9061; WMO 4902041) had a cumulative vertical profiling of 294 000 dbar ($\sim 292 \text{ km}$) over the course of 645 profiles in the Atlantic Ocean, and the longest-lived float (serial number 9023; WMO 4901726) survived for 415 days.

A critical aspect of the ALAMO is the air-deployment system, consisting of a 2.25 m parachute connected to the float by a water-activated release system and cardboard packaging held together by water soluble tape that restrains the foldable fins and provides shock absorption when the float strikes the sea surface. When the float submerges, a cornstarch collar within the water release dissolves, freeing a spring-driven pin, which detaches the air-deployment system from the float. While it is difficult to diagnose why a float fails without recovering it, circumstantial evidence can provide valuable insight. There are several modes of failure for the air-deployment sequence. First and foremost, the parachute must correctly inflate during the deployment sequence. To ensure that happens, a small drogue chute is deployed on release from the plane. Then, once the float reaches the ocean, the parachute and other packing materials must properly detach from the float without fouling; otherwise, the float will sink due to the additional weight of the parachute and water release.

In total, 60 ALAMO floats were deployed during the 2014–16 hurricane seasons. During the first year (2014), 6 of 10 floats (60%) worked on deployment. This relatively poor performance was traced back to the design of the parachutes and led to a reconfiguration of the air-deployment system. In 2015 the second year of the program, 27 of 30 floats (90%) worked upon deployment, and in the third year (2016), 19 of 20 floats (95%) worked. Since that improvement, the parachute system has not been further changed.

3. Example observations

The 2015 hurricane season was the most active on record for the central Pacific (between 140°W and the date line), with 16 tropical cyclones (Collins et al. 2016; Kruk et al. 2016). As a result, there were many AFRC WC-130J Hurricane Hunter flights through Pacific tropical systems to deploy ALAMOs for operational forecasting and observing the ocean’s response to the hurricanes.

To demonstrate typical data and their usage from an ALAMO float, we show the results from serial number 9077 (WMO 4902045), which was deployed on 3 August 2015 from an AFRC WC-130J through the internal AXBT chute in the eastern Pacific (EPAC) ahead of Hurricane Guillermo (Avila and Powell 2016). ALAMO 9077 subsequently came in close proximity to EPAC Hurricanes Hilda and Ignacio, CPAC Hurricane Oho, and EPAC Hurricane Olaf in sequence (Fig. 2; track information courtesy of the Hurricane Data second-generation database; Landsea and Franklin 2013). After an initial diagnostic dive, the float was programmed to profile

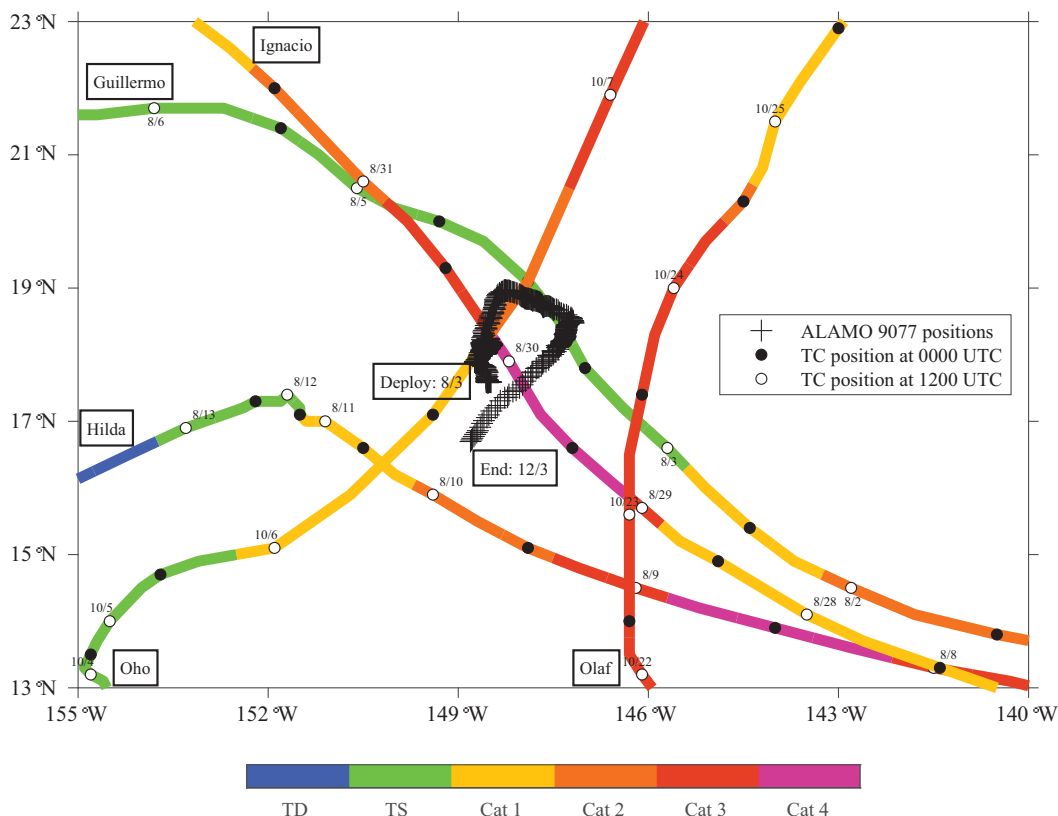


FIG. 2. The ALAMO float 9077 location relative to the paths of 2015 hurricanes Guillermo (CPA of 153 km at 0428 UTC 4 Aug), Hilda (CPA of 229 km at 1539 UTC 10 Aug), Ignacio (CPA of 17 km at 1611 UTC 30 Aug), Oho (CPA of 25 km at 0530 UTC 7 Oct), and Olaf (CPA of 143 km at 0611 UTC 24 Oct). ALAMO 9077 was deployed on 3 Aug and stopped reporting on 3 Dec. Hurricane track data are from the HURDAT2 database (Landsea and Franklin 2013). The hurricane tracks are color coded by intensity on the Saffir–Simpson scale from tropical depression (TD), tropical storm (TS), to hurricane categories 1 through 4.

13 times a day to a depth of approximately 300 dbar (Fig. 3a). During this rapid profiling sequence, the float descends as quickly as possible until it reaches the turnaround depth where it inflates the external bladder and rises to the surface (Fig. 3b). At its closest approach, Guillermo passed about 153 km from the float. The float continued in this mode until the hurricane moved out of the region and dissipated, whereupon the float was reprogrammed to profile 4 times a day to 300 dbar and remain in a park phase (drifting at 300 dbar to conserve battery power) between profiles (Fig. 3c). A few days later, on 7 August 2015, Hurricane Hilda began to rapidly intensify, becoming a major hurricane (Blake and Jelsema 2016a). During this period the float was returned to a rapid profiling mode of 13 profiles a day to 300 dbar. After Hilda weakened and passed 229 km from 9077, the float was again returned to profiling 4 times a day. Subsequently, Hurricane Ignacio formed and began to move toward the region, and the float was reprogrammed again to rapidly profile. Ignacio passed within 17 km of ALAMO float 9077 (Fig. 2) just after it reached its peak intensity as a category 4 hurricane with maximum winds of 65 m s^{-1} (Beven and Jacobson 2018). Later in the season, Hurricane Oho (Houston and Wroe

2016) developed and passed within 25 km of the float, followed by Hurricane Olaf (Blake and Jelsema 2016b), which passed 143 km from the float. After hurricane season, the float was programmed to profile daily to its maximum depth of 1100 dbar and park at 600 dbar (Fig. 3d). Over its 120-day mission, the float made 609 profiles, for a cumulative vertical profiling distance of 207 000 dbar ($\sim 206 \text{ km}$), before exhausting its batteries.

To demonstrate the utility of the in situ float observations, we compare the observations from ALAMO 9077 to select ocean metrics used in tropical cyclone forecasting (Fig. 4) diagnosed from the operational U.S. Navy Coupled Ocean Data Assimilation (NCODA) analysis system (Cummings 2005). In particular we compare the analyzed sea surface temperature, the depth of the 26°C isotherm, the tropical cyclone heat potential, and the average temperature of the upper 100 m (DeMaria et al. 2005; Price 2009). Note that the tropical cyclone heat potential here is defined as the vertical integral of the temperature above the 26°C isotherm relative to 26°C (Mainelli et al. 2008). Overall, NCODA tracks the observed ocean well, notably in the evolution of SST over the season (Fig. 4a). However, NCODA is not completely independent

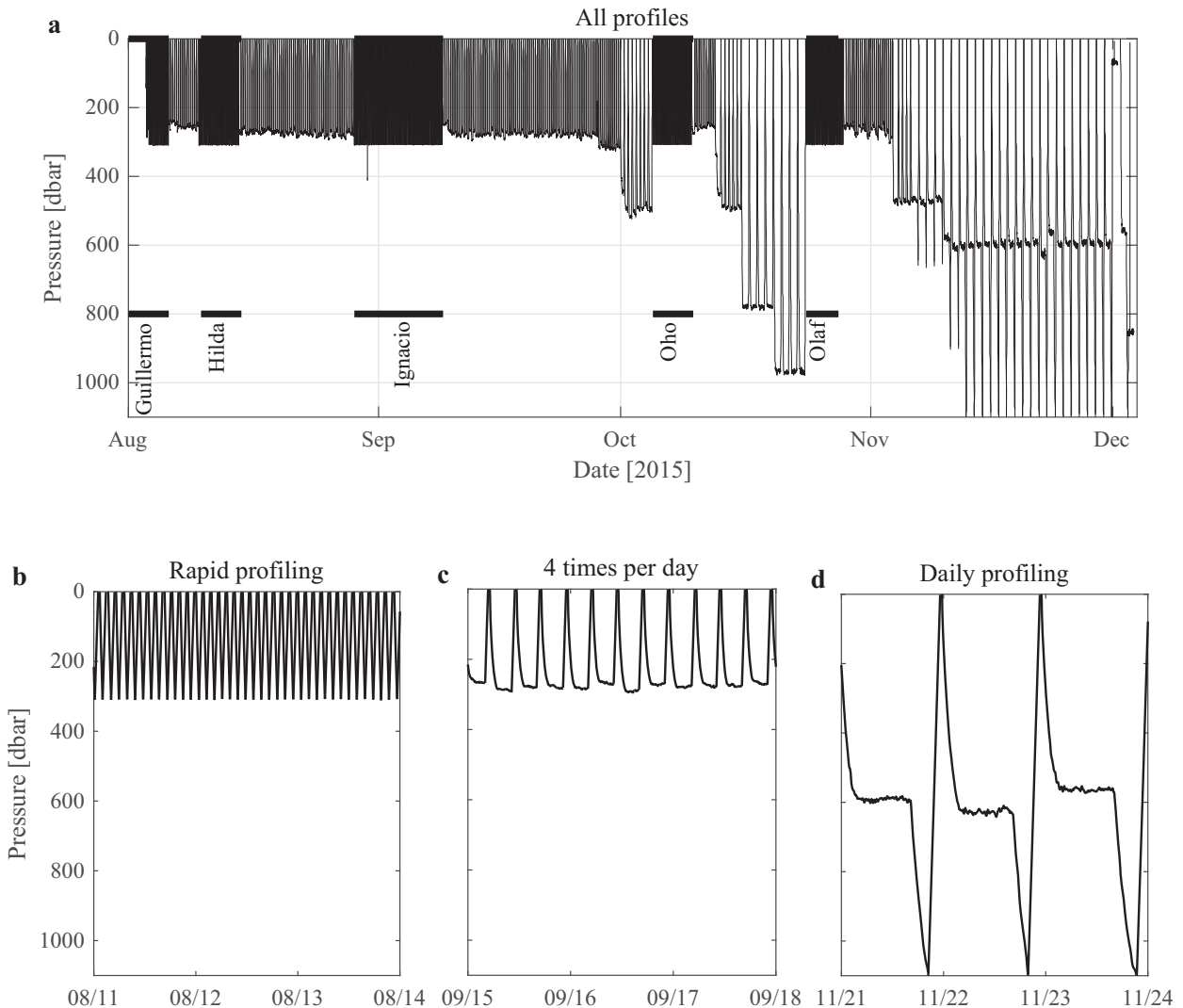


FIG. 3. Examples of different operational modes from ALAMO 9077: (a) all profiles plotted by depth and time, with near approach times of hurricanes annotated, (b) rapid profiling to 300 dbar, (c) profiling four times per day to 300 dbar and drifting at 300 dbar, and (d) daily profiling to 1100 dbar and drifting at 600 dbar.

of the observations, as the ALAMO data were distributed on the GTS and therefore available for assimilation into the model. Perhaps the most notable aspect is the strong, high-frequency variability in the depth of the 26°C isotherm and in the tropical cyclone heat potential observed by the float that is averaged out by the daily NCODA analysis. In this region, there is vigorous internal wave activity associated with the semidiurnal internal tides generated by the Hawaiian Ridge (Merrifield et al. 2001), which induces large heaving of the 26°C isotherm, and the diagnosed tropical cyclone heat potential.

Finally, we briefly focus on a few aspects of the observed ocean response to passage of Hurricane Ignacio. The entire ocean temperature record observed by the float is shown in Fig. 5. Prior to the passage of the tropical cyclone there is the variability associated with the internal tides. Then the passage of

Ignacio induced a strong ocean response: a strong initial downwelling event depressed the 26°C isotherm depth by 40 m (Fig. 4c), followed by upwelling, inertial oscillations and mixing in the upper ocean (Fig. 5b). These observations show the utility of having persistent monitoring of the upper ocean, before, during and after the passage of the tropical cyclone. A single AXBT profile would give an incomplete view and not capture the details of rapid ocean response, and given the inherent background ocean variability, could give a strongly biased view of the ocean's interaction with the tropical cyclone.

4. Discussion

The development and demonstration of A-sized air-deployable profiling floats has enabled sustained ocean observations during operational AFRC Hurricane Hunter reconnaissance flights. The

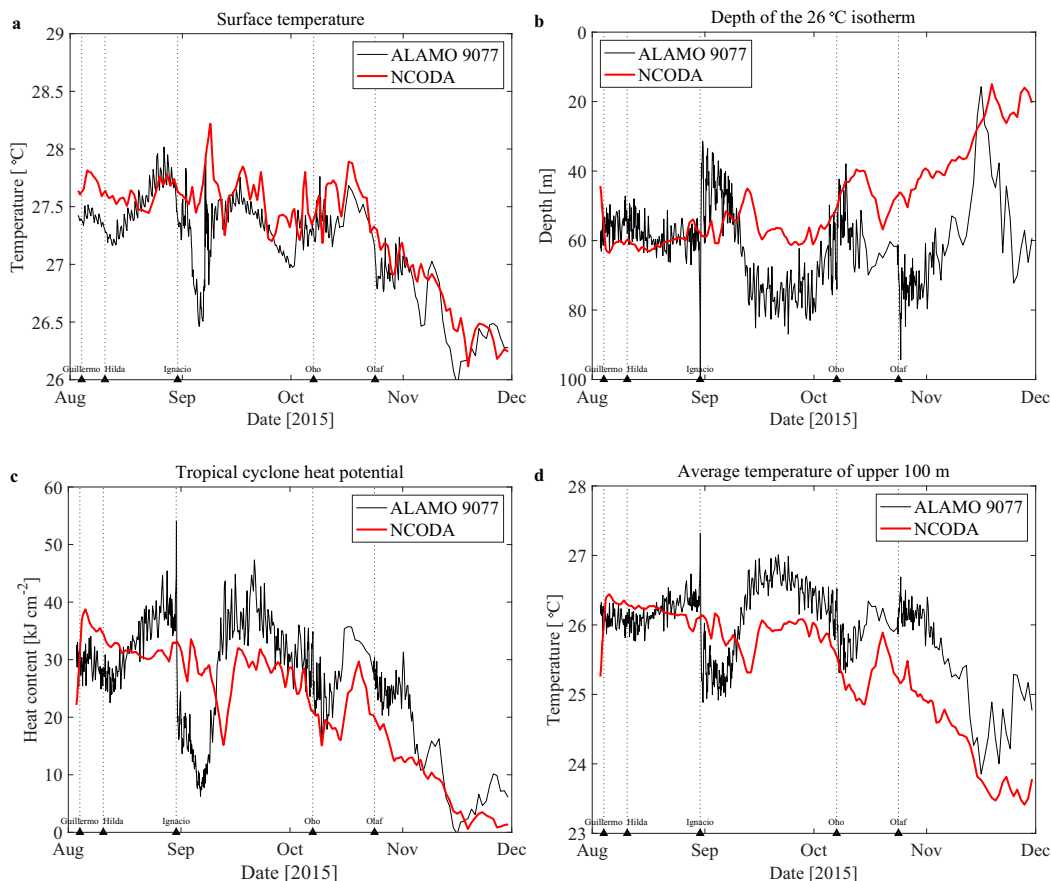


FIG. 4. Metrics comparing the NCODA analysis to observations from ALAMO 9077: (a) the sea surface temperature ($^{\circ}\text{C}$), (b) depth of the 26°C isotherm (m), (c) tropical cyclone heat potential (kJ cm^{-2}), and (d) average temperature of the upper 100 m ($^{\circ}\text{C}$). Small triangles with gray dotted lines and hurricane names along the time axis indicate time of closest point of approach between the float and each storm.

relative ease of deployment provides targeted ocean observations around a tropical cyclone that would be difficult to obtain otherwise. We expect that the ALAMO will find widespread use among the oceanographic community. Given their versatility and diminutive size, they are easily deployed from various aircraft and adaptable to users' needs.

Beginning in 2017, ALAMO floats with pressure, temperature, and salinity sensors (CTDs), both the RBRargo³ inductive CTD (Halverson et al. 2020) and the Sea-Bird CP41+ (Johnson et al. 2007) have been deployed from operational reconnaissance flights. These temperature and salinity profiles show the importance that stratification can play in the ocean's response to a hurricane (Sanabia and Jayne 2020).

Beyond tropical cyclone research, ALAMO floats have also been air deployed in the Chukchi Sea region of the Arctic Ocean for the Arctic Heat program to provide sustained observations in the challenging marginal ice zone (Wood et al. 2018). The ROSETTA observational program utilized ALAMO floats to make measurements of seasonal to interannual variability in upper-ocean hydrography over the seasonally ice-covered Ross Sea continental shelf (Porter et al. 2019). Finally ALAMO

observations have been collected in the Northern Arabian Sea as part of the Northern Arabian Sea Circulation–autonomous research program (NASCar; Centurioni et al. 2017) and the Monsoon Intraseasonal Oscillations in the Tropical Indian Ocean and the Bay of Bengal (MISO-BoB; Shroyer et al. 2021) to understand the rapid evolution of the upper Indian Ocean during the monsoons.

Acknowledgments. The authors are deeply indebted to the U.S. Air Force Reserve 53rd Weather Reconnaissance Squadron, the pilots, navigators, weather officers, load masters, and crew chiefs, for their enthusiastic support of the testing and deployments of the floats. Jim Dufour was integral to the inception and design of the ALAMO float, and his enthusiastic support of the program is gratefully acknowledged. Jeff Kerling from the Naval Oceanographic Office provided continuous encouragement and logistical guidance. This work was supported by the National Oceanographic and Atmospheric Administration under Grants NA13OAR4830233 (as part of CINAR Sandy Supplemental funding from the Disaster Relief Appropriations Act of 2013) and NA14OAR4320158 and by

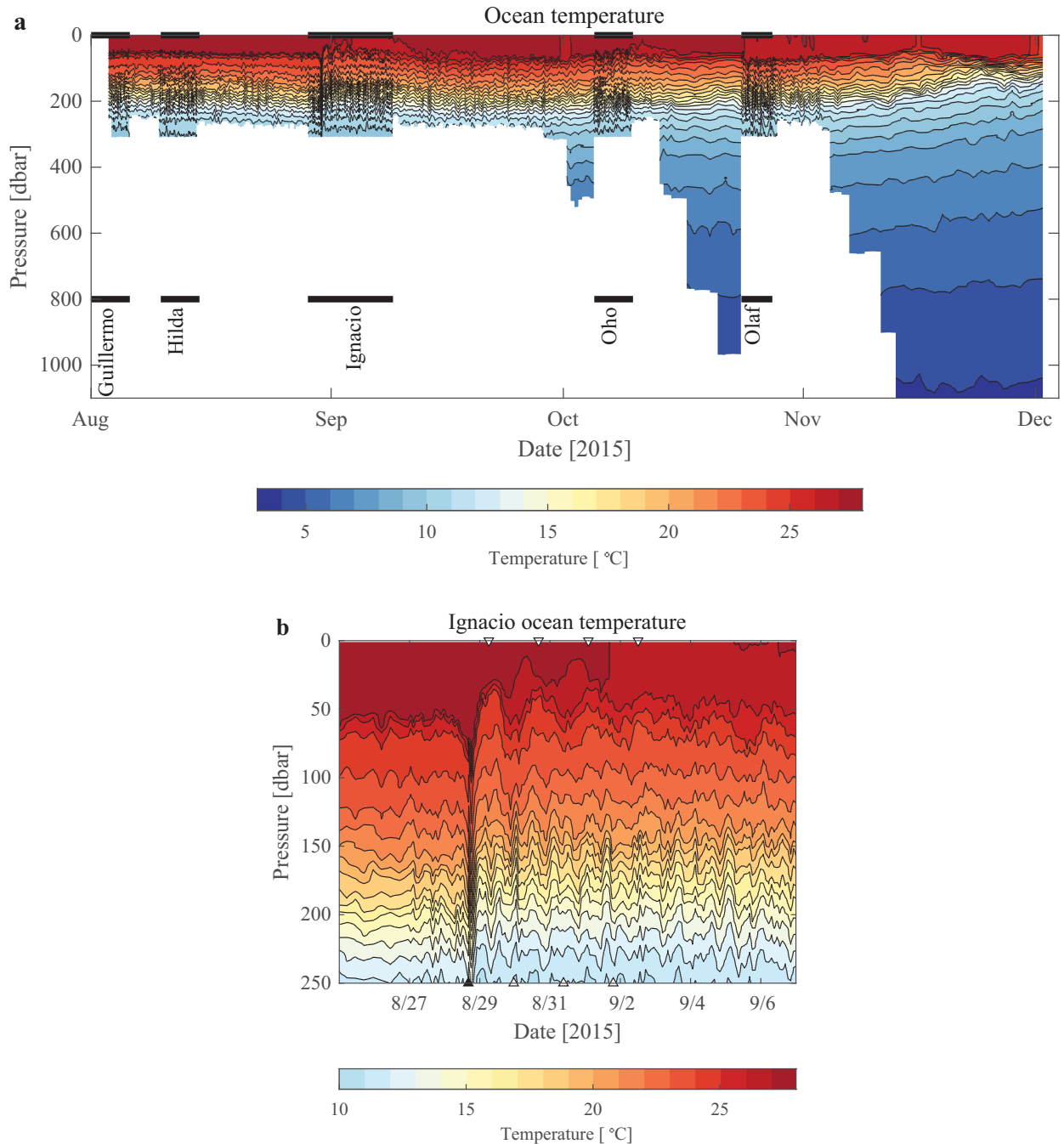


FIG. 5. (a) The full temperature record from ALAMO 9077, showing the variability due to internal tides along with the upper-ocean response to passing tropical cyclones, with near approach times of each storm annotated. (b) Focused view on the period of Hurricane Ignacio's passage showing a strong ocean response to the hurricane with a notable downwelling of the isotherms, followed by strong inertial waves along with mixing and cooling in the surface ocean. The small black point on the lower axis indicates time of closest point of approach between the float and Ignacio. Small white triangles along the upper axis correspond to times of the first few crests of the inertial oscillations, and the small white triangles along the lower axis correspond to the first few troughs.

Office of Naval Research under Grants N0001416WX01384, N0001416WX01262, and N000141512293. ALAMO floats are commercially available from MRV Systems, LLC (<https://www.mrvsys.com>).

Data availability statement. Plots and data from the ALAMO floats, as well as maps of deployment locations, can be seen at <https://argo.whoi.edu/alamo>, and archived quality-controlled float data are available at <https://accession.nodc>.

noaa.gov/0210577. The HURDAT database is available at https://www.aoml.noaa.gov/hrd/hurdat/Data_Storm.html. The NCODA ocean metrics are available at https://www.nrlmry.navy.mil/atcf_web/nopp_ohc.

REFERENCES

- Alaka, G. J., Jr., D. Sheinin, B. Thomas, L. Gramer, Z. Zhang, B. Liu, H.-S. Kim, and A. Mehra, 2020: A hydrodynamical atmosphere/ocean coupled modeling system for multiple tropical cyclones. *Atmosphere*, **11**, 869, <https://doi.org/10.3390/atmos11080869>.
- Avila, L. A., and J. Powell, 2016: Tropical cyclone report: Hurricane Guillermo. National Hurricane Center Tech. Rep. EP092015, 16 pp., https://www.nhc.noaa.gov/data/tcr/EP092015_Guillermo.pdf.
- Balaguru, K., S. Taraphdar, L. R. Leung, G. R. Foltz, and J. A. Knaff, 2014: Cyclone-cyclone interactions through the ocean pathway. *Geophys. Res. Lett.*, **41**, 6855–6862, <https://doi.org/10.1002/2014GL061489>.
- , G. R. Foltz, L. R. Leung, E. D’Asaro, K. A. Emanuel, H. Liu, and S. E. Zedler, 2015: Dynamic potential intensity: An improved representation of the ocean’s impact on tropical cyclones. *Geophys. Res. Lett.*, **42**, 6739–6746, <https://doi.org/10.1002/2015GL064822>.
- , —, —, S. M. Hagos, and D. R. Judi, 2018: On the use of ocean dynamic temperature for hurricane intensity forecasting. *Wea. Forecasting*, **33**, 411–418, <https://doi.org/10.1175/WAF-D-17-0143.1>.
- Baranowski, D. B., P. J. Falta, S. Chen, and P. G. Black, 2014: Upper ocean response to the passage of two sequential typhoons. *Ocean Sci.*, **10**, 559–570, <https://doi.org/10.5194/os-10-559-2014>.
- Beven, J. L., II, and C. Jacobson, 2018: Tropical cyclone report: Hurricane Ignacio. National Hurricane Center Tech. Rep. EP122015, 19 pp., https://www.nhc.noaa.gov/data/tcr/EP122015_Ignacio.pdf.
- Black, P. G., and Coauthors, 2007: Air–sea exchange in hurricanes: Synthesis of observations from the Coupled Boundary Layer Air–Sea Transfer experiment. *Bull. Amer. Meteor. Soc.*, **88**, 357–374, <https://doi.org/10.1175/BAMS-88-3-357>.
- Blake, E. S., and J. Jelsema, 2016a: Tropical cyclone report: Hurricane Hilda. National Hurricane Center Tech. Rep. EP102015, 16 pp., https://www.nhc.noaa.gov/data/tcr/EP102015_Hilda.pdf.
- , and —, 2016b: Tropical cyclone report: Hurricane Olaf. National Hurricane Center Tech. Rep. EP192015, 17 pp., https://www.nhc.noaa.gov/data/tcr/EP192015_Olaf.pdf.
- Bosart, L. F., W. E. Bracken, J. Molinari, C. S. Velden, and P. G. Black, 2000: Environmental influences on the rapid intensification of Hurricane Opal (1995) over the Gulf of Mexico. *Mon. Wea. Rev.*, **128**, 322–352, [https://doi.org/10.1175/1520-0493\(2000\)128<0322:EIOTRI>2.0.CO;2](https://doi.org/10.1175/1520-0493(2000)128<0322:EIOTRI>2.0.CO;2).
- Brand, S., 1971: The effects on a tropical cyclone of cooler surface waters due to upwelling and mixing produced by a prior tropical cyclone. *J. Appl. Meteor. Climatol.*, **10**, 865–874, [https://doi.org/10.1175/1520-0450\(1971\)010<0865:TEOATC>2.0.CO;2](https://doi.org/10.1175/1520-0450(1971)010<0865:TEOATC>2.0.CO;2).
- Byers, H. R., 1944: *General Meteorology*. McGraw-Hill, 645 pp.
- Cangialosi, J. P., E. Blake, M. DeMaria, A. Penny, A. Latta, E. Rappaport, and V. Tallapragada, 2020: Recent progress in tropical cyclone intensity forecasting at the National Hurricane Center. *Wea. Forecasting*, **35**, 1913–1922, <https://doi.org/10.1175/WAF-D-20-0059.1>.
- Carnes, M. R., J. L. Mitchell, and P. W. Dewitt, 1990: Synthetic temperature profiles derived from Geosat altimetry: Comparison with air-dropped expendable bathythermograph profiles. *J. Geophys. Res.*, **95**, 17979–17992, <https://doi.org/10.1029/JC095iC10p17979>.
- Centurioni, L. R., and Coauthors, 2017: Northern Arabian Sea Circulation-Autonomous Research (NASCar): A research initiative based on autonomous sensors. *Oceanography*, **30** (2), 74–87, <https://doi.org/10.5670/oceanog.2017.224>.
- Chang, S. W., and R. A. Anthes, 1978: Numerical simulations of the ocean’s nonlinear, baroclinic response to translating hurricanes. *J. Phys. Oceanogr.*, **8**, 468–480, [https://doi.org/10.1175/1520-0485\(1978\)008<0468:NSOTON>2.0.CO;2](https://doi.org/10.1175/1520-0485(1978)008<0468:NSOTON>2.0.CO;2).
- Chen, S., J. A. Cummings, J. M. Schmidt, E. R. Sanabia, and S. R. Jayne, 2017a: Targeted ocean sampling guidance for tropical cyclones. *J. Geophys. Res. Oceans*, **122**, 3505–3518, <https://doi.org/10.1002/2017JC012727>.
- , R. L. Elsberry, and P. A. Harr, 2017b: Modeling interaction of a tropical cyclone with its cold wake. *J. Atmos. Sci.*, **74**, 3981–4001, <https://doi.org/10.1175/JAS-D-16-0246.1>.
- Cheng, L., J. Zhu, and R. L. Sriver, 2015: Global representation of tropical cyclone-induced short-term ocean thermal changes using Argo data. *Ocean Sci.*, **11**, 719–741, <https://doi.org/10.5194/os-11-719-2015>.
- , and Coauthors, 2016: XBT science: Assessment of instrumental biases and errors. *Bull. Amer. Meteor. Soc.*, **97**, 924–933, <https://doi.org/10.1175/BAMS-D-15-00031.1>.
- Cione, J. J., 2015: The relative roles of the ocean and atmosphere as revealed by buoy air–sea observations in hurricanes. *Mon. Wea. Rev.*, **143**, 904–913, <https://doi.org/10.1175/MWR-D-13-00380.1>.
- , and E. W. Uhlhorn, 2003: Sea surface temperature variability in hurricanes: Implications with respect to intensity change. *Mon. Wea. Rev.*, **131**, 1783–1796, <https://doi.org/10.1175/2562.1>.
- Collins, J. M., P. J. Klotzbach, R. N. Maue, D. R. Roache, E. S. Blake, C. H. Paxton, and C. A. Mehta, 2016: The record-breaking 2015 hurricane season in the eastern North Pacific: An analysis of environmental conditions. *Geophys. Res. Lett.*, **43**, 9217–9224, <https://doi.org/10.1002/2016GL070597>.
- Cummings, J. A., 2005: Operational multivariate ocean data assimilation. *Quart. J. Roy. Meteor. Soc.*, **131**, 3583–3604, <https://doi.org/10.1256/qj.05.105>.
- D’Asaro, E. A., T. B. Sanford, P. P. Niiler, and E. J. Terrill, 2007: Cold wake of Hurricane Frances. *Geophys. Res. Lett.*, **34**, L15609, <https://doi.org/10.1029/2007GL030160>.
- , and Coauthors, 2011: Typhoon-ocean interaction in the western North Pacific: Part 1. *Oceanography*, **24** (4), 24–31, <https://doi.org/10.5670/oceanog.2011.91>.
- , and Coauthors, 2014: Impact of typhoons on the ocean in the Pacific. *Bull. Amer. Meteor. Soc.*, **95**, 1405–1418, <https://doi.org/10.1175/BAMS-D-12-00104.1>.
- Davis, R. E., D. C. Webb, L. A. Regier, and J. Dufour, 1992: The Autonomous Lagrangian Circulation Explorer (ALACE). *J. Atmos. Oceanic Technol.*, **9**, 264–285, [https://doi.org/10.1175/1520-0426\(1992\)009<0264:TALCE>2.0.CO;2](https://doi.org/10.1175/1520-0426(1992)009<0264:TALCE>2.0.CO;2).
- , T. J. Sherman, and J. Dufour, 2001: Profiling ALACEs and other advances in autonomous subsurface floats. *J. Atmos. Oceanic Technol.*, **18**, 982–993, [https://doi.org/10.1175/1520-0426\(2001\)018<0982:PAAOAI>2.0.CO;2](https://doi.org/10.1175/1520-0426(2001)018<0982:PAAOAI>2.0.CO;2).
- DeMaria, M., and J. Kaplan, 1994: A Statistical Hurricane Intensity Prediction Scheme (SHIPS) for the Atlantic basin. *Wea.*

- Forecasting, **9**, 209–220, [https://doi.org/10.1175/1520-0434\(1994\)009<0209:ASHIPS>2.0.CO;2](https://doi.org/10.1175/1520-0434(1994)009<0209:ASHIPS>2.0.CO;2).
- , M. Mainelli, L. K. Shay, J. A. Knaff, and J. Kaplan, 2005: Further improvements to the Statistical Hurricane Intensity Prediction Scheme (SHIPS). *Wea. Forecasting*, **20**, 531–543, <https://doi.org/10.1175/WAF862.1>.
- , J. A. Knaff, and C. Sampson, 2007: Evaluation of the long-term trends in tropical cyclone intensity forecast. *Meteor. Atmos. Phys.*, **97**, 19–28, <https://doi.org/10.1007/s00703-006-0241-4>.
- , C. R. Sampson, J. A. Knaff, and M. D. Musgrave, 2014: Is tropical cyclone intensity guidance improving? *Bull. Amer. Meteor. Soc.*, **95**, 387–398, <https://doi.org/10.1175/BAMS-D-12-00240.1>.
- Doyle, J. D., and Coauthors, 2014: Tropical cyclone prediction using COAMPS-TC. *Oceanography*, **27** (3), 104–115, <https://doi.org/10.5670/oceanog.2014.72>.
- Dufour, J. E., and B. K. Newville, 2017: Controlling buoyancy of an underwater vehicle using a dual-internal-reservoir configuration to enhance efficiency of inflating and deflating an external chamber. U.S. Patent 9550 554 B2, 13 pp.
- , and —, 2018: Air-based-deployment-compatible underwater vehicle configured to perform vertical profiling and, during information transmission, perform motion stabilization at a water surface, and associated methods. U.S. Patent 9884670 B2, 21 pp.
- Emanuel, K., 2004: Tropical cyclone energetics and structure. *Atmospheric Turbulence and Mesoscale Meteorology: Scientific Research Inspired by Doug Lilly*, E. Fedorovich, R. Rotunno, and B. Stevens, Eds., Cambridge University Press, 165–192, <https://doi.org/10.1017/CBO9780511735035.010>.
- , C. DesAutels, C. Holloway, and R. Korty, 2004: Environmental control of tropical cyclone intensity. *J. Atmos. Sci.*, **61**, 843–858, [https://doi.org/10.1175/1520-0469\(2004\)061<0843:ECOTCI>2.0.CO;2](https://doi.org/10.1175/1520-0469(2004)061<0843:ECOTCI>2.0.CO;2).
- Fisher, E. L., 1958: Hurricanes and the sea-surface temperature field. *J. Meteor.*, **15**, 328–333, [https://doi.org/10.1175/1520-0469\(1958\)015<0328:HATSST>2.0.CO;2](https://doi.org/10.1175/1520-0469(1958)015<0328:HATSST>2.0.CO;2).
- Gall, R., J. Franklin, F. Marks, E. N. Rappaport, and F. Toepfer, 2013: The Hurricane Forecast Improvement Project. *Bull. Amer. Meteor. Soc.*, **94**, 329–343, <https://doi.org/10.1175/BAMS-D-12-00071.1>.
- Gill, A. E., 1982: *Atmosphere-Ocean Dynamics*. Academic Press, 662 pp.
- Goni, G., and J. A. Trinanes, 2003: Ocean thermal structure monitoring could aid in the intensity forecast of tropical cyclones. *Eos, Trans. Amer. Geophys. Union*, **84**, 573–578, <https://doi.org/10.1029/2003EO510001>.
- , and Coauthors, 2009: Applications of satellite-derived ocean measurements to tropical cyclone intensity forecasting. *Oceanography*, **22** (3), 190–197, <https://doi.org/10.5670/oceanog.2009.78>.
- Gopalakrishnan, S., and Coauthors, 2020: 2020 HFIP R&D activities summary: Recent results and operational implementation. NOAA HFIP Tech. Rep. HFIP2021-1, 49 pp., https://hfip.org/sites/default/files/documents/hfip-annual-report-2020-final_0.pdf.
- Gould, W. J., 2005: From Swallow floats to Argo—The development of neutrally buoyant floats. *Deep-Sea Res. II*, **52**, 529–543, <https://doi.org/10.1016/j.dsr2.2004.12.005>.
- Gray, M., 1979: Hurricanes: Their formation, structure, and likely role in the tropical circulation. *Meteorology over the Tropical Oceans*, D. B. Shaw, Ed., Royal Meteorological Society, 155–218.
- Halliwel, G. R., Jr., L. K. Shay, S. D. Jacob, O. M. Smedstad, and E. W. Uhlhorn, 2008: Improving ocean model initialization for coupled tropical cyclone forecast models using GODAE nowcasts. *Mon. Wea. Rev.*, **136**, 2576–2591, <https://doi.org/10.1175/2007MWR2154.1>.
- , —, J. K. Brewster, and W. J. Teague, 2011: Evaluation and sensitivity analysis of an ocean model response to Hurricane Ivan. *Mon. Wea. Rev.*, **139**, 921–945, <https://doi.org/10.1175/2010MWR3104.1>.
- , S. Gopalakrishnan, F. Marks, and D. Willey, 2015: Idealized study of ocean impacts on tropical cyclone intensity forecasts. *Mon. Wea. Rev.*, **143**, 1142–1165, <https://doi.org/10.1175/MWR-D-14-00022.1>.
- Halverson, M., E. Siegel, and G. Johnson, 2020: Inductive-conductivity cell. *Sea Technology*, Vol. 61 (2), 24–27.
- Heinmiller, R. H., C. C. Ebbesmeyer, B. A. Taft, D. B. Olson, and O. P. Nikitin, 1983: Systematic errors in expendable bathythermograph (XBT) profiles. *Deep-Sea Res.*, **30**, 1185–1196, [https://doi.org/10.1016/0198-0149\(83\)90096-1](https://doi.org/10.1016/0198-0149(83)90096-1).
- Hendricks, E. A., M. S. Peng, B. Fu, and T. Li, 2010: Quantifying environmental control on tropical cyclone intensity change. *Mon. Wea. Rev.*, **138**, 3243–3271, <https://doi.org/10.1175/2010MWR3185.1>.
- Houston, S., and D. Wroe, 2016: Tropical cyclone report: Hurricane Oho. Central Pacific Hurricane Center Tech. Rep. CP072015, 9 pp., https://www.nhc.noaa.gov/data/tcr/CP072015_Oho.pdf.
- IOOC, 2004: Interagency Ocean Observation Committee technical workshop on applications of Iridium telecommunications to oceanographic and polar research. IOOC Tech. Rep. 13, 40 pp., <https://www.iooc.us/wp-content/uploads/2010/12/13.pdf>.
- Ito, K., T. Kuroda, and K. Saito, 2015: Forecasting a large number of tropical cyclone intensities around Japan using a high-resolution atmosphere–ocean coupled model. *Wea. Forecasting*, **30**, 793–808, <https://doi.org/10.1175/WAF-D-14-00034.1>.
- Johnson, G. C., J. M. Toole, and N. G. Larson, 2007: Sensor corrections for Sea-Bird SBE-41CP and SBE-41 CTDs. *J. Atmos. Oceanic Technol.*, **24**, 1117–1130, <https://doi.org/10.1175/JTECH2016.1>.
- Johnston, T. M. S., S. Wang, C.-Y. Lee, J. M. Moum, D. L. Rudnick, and A. Sobel, 2021: Near-inertial wave propagation in the wake of Super Typhoon Mangkhut: Measurements from a profiling float array. *J. Geophys. Res. Oceans*, **126**, e2020JC016749, <https://doi.org/10.1029/2020JC016749>.
- Kaplan, J., and M. DeMaria, 2003: Large-scale characteristics of rapidly intensifying tropical cyclones in the North Atlantic basin. *Wea. Forecasting*, **18**, 1093–1108, [https://doi.org/10.1175/1520-0434\(2003\)018<1093:LCORIT>2.0.CO;2](https://doi.org/10.1175/1520-0434(2003)018<1093:LCORIT>2.0.CO;2).
- Karnauskas, K. B., L. Zhang, and K. A. Emanuel, 2021: The feedback of cold wakes on tropical cyclones. *Geophys. Res. Lett.*, **48**, e2020GL091676, <https://doi.org/10.1029/2020GL091676>.
- Kimberlain, T. B., and M. J. Brennan, 2017: Tropical cyclone motion. *Global Guide to Tropical Cyclone Forecasting*, C. J. Guard, Ed., World Meteorological Organization, 63–125, <https://cyclone.wmo.int/pdf/Chapter-Three.pdf>.
- Knaff, J. A., M. DeMaria, C. R. Sampson, J. E. Peak, J. Cummings, and W. H. Schubert, 2013: Upper oceanic energy response to tropical cyclone passage. *J. Climate*, **26**, 2631–2650, <https://doi.org/10.1175/JCLI-D-12-00038.1>.

- Kossin, J. P., 2017: Hurricane intensification along United States coast suppressed during active hurricane periods. *Nature*, **541**, 390–393, <https://doi.org/10.1038/nature20783>.
- Kruk, M. C., C. J. Schreck, and T. Evans, 2016: Tropical cyclones: Eastern North Pacific and central North Pacific basins. *Bull. Amer. Meteor. Soc.*, **97**, S108–S110.
- Landsea, C. W., and J. L. Franklin, 2013: Atlantic hurricane database uncertainty and presentation of a new database format. *Mon. Wea. Rev.*, **141**, 3576–3592, <https://doi.org/10.1175/MWR-D-12-00254.1>.
- Legler, D. M., and Coauthors, 2015: The current status of the real-time in situ Global Ocean Observing System for operational oceanography. *J. Oper. Oceanogr.*, **8** (Suppl.), s189–s200, <https://doi.org/10.1080/1755876X.2015.1049883>.
- Leipper, D. F., 1967: Observed ocean conditions and Hurricane Hilda, 1964. *J. Atmos. Sci.*, **24**, 182–186, [https://doi.org/10.1175/1520-0469\(1967\)024<0182:OOCANH>2.0.CO;2](https://doi.org/10.1175/1520-0469(1967)024<0182:OOCANH>2.0.CO;2).
- , and D. Volgenau, 1972: Hurricane heat potential of the Gulf of Mexico. *J. Phys. Oceanogr.*, **2**, 218–224, [https://doi.org/10.1175/1520-0485\(1972\)002<0218:HHPOTG>2.0.CO;2](https://doi.org/10.1175/1520-0485(1972)002<0218:HHPOTG>2.0.CO;2).
- Lin, I.-I., C.-H. Chen, I.-F. Pun, W. T. Liu, and C.-C. Wu, 2009: Warm ocean anomaly, air sea fluxes, and the rapid intensification of Tropical Cyclone Nargis (2008). *Geophys. Res. Lett.*, **36**, L03817, <https://doi.org/10.1029/2008GL035815>.
- , G. J. Goni, J. A. Knaff, C. Forbes, and M. M. Ali, 2013a: Ocean heat content for tropical cyclone intensity forecasting and its impact on storm surge. *Nat. Hazards*, **66**, 1481–1500, <https://doi.org/10.1007/s11069-012-0214-5>.
- , and Coauthors, 2013b: An ocean coupling potential intensity index for tropical cyclones. *Geophys. Res. Lett.*, **40**, 1878–1882, <https://doi.org/10.1002/grl.50091>.
- Mainelli, M., M. DeMaria, L. K. Shay, and G. Goni, 2008: Application of oceanic heat content estimation to operational forecasting of recent Atlantic category 5 hurricanes. *Wea. Forecasting*, **23**, 3–16, <https://doi.org/10.1175/2007WAF2006111.1>.
- Malkus, J. S., and H. Riehl, 1960: On the dynamics and energy transformations in steady-state hurricanes. *Tellus*, **12**, 1–20, <https://doi.org/10.3402/tellusa.v12i1.9351>.
- Marks, F. D., and Coauthors, 1998: Landfalling tropical cyclones: Forecast problems and associated research opportunities. *Bull. Amer. Meteor. Soc.*, **79**, 305–323, [https://doi.org/10.1175/1520-0477\(1998\)079<0305:LTCFPA>2.0.CO;2](https://doi.org/10.1175/1520-0477(1998)079<0305:LTCFPA>2.0.CO;2).
- Merrifield, M. A., P. E. Holloway, and T. M. S. Johnston, 2001: The generation of internal tides at the Hawaiian Ridge. *Geophys. Res. Lett.*, **28**, 559–562, <https://doi.org/10.1029/2000GL011749>.
- Meyers, P. C., L. K. Shay, and J. K. Brewster, 2014: Development and analysis of the systematically merged Atlantic regional temperature and salinity climatology for oceanic heat content estimates. *J. Atmos. Oceanic Technol.*, **31**, 131–149, <https://doi.org/10.1175/JTECH-D-13-00100.1>.
- Miles, T., G. Seroka, and S. Glenn, 2017: Coastal ocean circulation during Hurricane Sandy. *J. Geophys. Res. Oceans*, **122**, 7095–7114, <https://doi.org/10.1002/2017JC013031>.
- Mogensen, K. S., L. Magnusson, and J.-R. Bidlot, 2017: Tropical cyclone sensitivity to ocean coupling in the ECMWF coupled model. *J. Geophys. Res. Oceans*, **122**, 4392–4412, <https://doi.org/10.1002/2017JC012753>.
- Mrvaljevic, R. K., and Coauthors, 2013: Observations of the cold wake of Typhoon Fanapi (2010). *Geophys. Res. Lett.*, **40**, 316–321, <https://doi.org/10.1029/2012GL054282>.
- Nelson, N. B., 1998: Spatial and temporal extent of sea surface temperature modifications by hurricanes in the Sargasso Sea during the 1995 season. *Mon. Wea. Rev.*, **126**, 1364–1368, [https://doi.org/10.1175/1520-0493\(1998\)126<1364:SATEOS>2.0.CO;2](https://doi.org/10.1175/1520-0493(1998)126<1364:SATEOS>2.0.CO;2).
- Palmén, E. H., 1948: On the formation and structure of tropical hurricanes. *Geophysica*, **3**, 26–38.
- Park, J. J., Y.-O. Kwon, and J. F. Price, 2011: Argo array observation of ocean heat content changes induced by tropical cyclones in the North Pacific. *J. Geophys. Res.*, **116**, C12025, <https://doi.org/10.1029/2011JC007165>.
- Porter, D. F., and Coauthors, 2019: Evolution of the seasonal surface mixed layer of the Ross Sea, Antarctica, observed with autonomous profiling floats. *J. Geophys. Res. Oceans*, **124**, 4934–4953, <https://doi.org/10.1029/2018JC014683>.
- Price, J. F., 1981: Upper ocean response to a hurricane. *J. Phys. Oceanogr.*, **11**, 153–175, [https://doi.org/10.1175/1520-0485\(1981\)011<0153:UORTAH>2.0.CO;2](https://doi.org/10.1175/1520-0485(1981)011<0153:UORTAH>2.0.CO;2).
- , 2009: Metrics of hurricane-ocean interaction: Vertically-integrated or vertically-averaged ocean temperature? *Ocean Sci.*, **5**, 351–368, <https://doi.org/10.5194/os-5-351-2009>.
- Pun, I.-F., J. F. Price, and S. R. Jayne, 2016: Satellite-derived ocean thermal structure from the North Atlantic hurricane season. *Mon. Wea. Rev.*, **144**, 877–896, <https://doi.org/10.1175/MWR-D-15-0275.1>.
- Rappaport, E. N., and Coauthors, 2009: Advances and challenges at the National Hurricane Center. *Wea. Forecasting*, **24**, 395–419, <https://doi.org/10.1175/2008WAF2222128.1>.
- , J.-G. Jiing, and C. W. Landsea, 2012: The Joint Hurricane Test Bed: Its first decade of tropical cyclone research-to-operations activities reviewed. *Bull. Amer. Meteor. Soc.*, **93**, 371–380, <https://doi.org/10.1175/BAMS-D-11-00037.1>.
- Riehl, H., 1950: A model of hurricane formation. *J. Appl. Phys.*, **21**, 917–925, <https://doi.org/10.1063/1.1699784>.
- Riser, S. C., and Coauthors, 2016: Fifteen years of ocean observations with the global Argo array. *Nat. Climate Change*, **6**, 145–153, <https://doi.org/10.1038/nclimate2872>.
- , D. Swift, and R. Drucker, 2018: Profiling floats in SOCOM: Technical capabilities for studying the Southern Ocean. *J. Geophys. Res. Oceans*, **123**, 4055–4073, <https://doi.org/10.1002/2017JC013419>.
- Roemmich, D., and B. Cornuelle, 1987: Digitization and calibration of the expendable bathythermograph. *Deep-Sea Res.*, **34**, 299–307, [https://doi.org/10.1016/0198-0149\(87\)90088-4](https://doi.org/10.1016/0198-0149(87)90088-4).
- , and Coauthors, 2009: The Argo program: Observing the global ocean with profiling floats. *Oceanography*, **22** (2), 34–43, <https://doi.org/10.5670/oceanog.2009.36>.
- , and Coauthors, 2019: Deep SOLO: A full-depth profiling float for the Argo program. *J. Atmos. Oceanic Technol.*, **36**, 1967–1981, <https://doi.org/10.1175/JTECH-D-19-0066.1>.
- Sanabia, E. R., and S. R. Jayne, 2020: Ocean observations under two major hurricanes: Evolution of the response across the storm wakes. *AGU Adv.*, **1**, e2019AV000161, <https://doi.org/10.1029/2019AV000161>.
- , B. S. Barrett, P. G. Black, S. Chen, and J. A. Cummings, 2013: Real-time upper-ocean temperature observations from aircraft during operational hurricane reconnaissance missions: AXBT demonstration project year one results. *Wea. Forecasting*, **28**, 1404–1422, <https://doi.org/10.1175/WAF-D-12-00107.1>.
- Sanders, F., and J. R. Gyakum, 1980: Synoptic-dynamic climatology of the “bomb.” *Mon. Wea. Rev.*, **108**, 1589–1606, [https://doi.org/10.1175/1520-0493\(1980\)108<1589:SDCOT>2.0.CO;2](https://doi.org/10.1175/1520-0493(1980)108<1589:SDCOT>2.0.CO;2).
- Sanford, T. B., J. F. Price, J. B. Girtton, and D. C. Webb, 2007: Highly resolved observations and simulations of the ocean

- response to a hurricane. *Geophys. Res. Lett.*, **34**, L13604, <https://doi.org/10.1029/2007GL029679>.
- , —, and —, 2011: Upper ocean response to Hurricane Frances (2004) observed by profiling EM-APEX floats. *J. Phys. Oceanogr.*, **41**, 1041–1056, <https://doi.org/10.1175/2010JPO4313.1>.
- Seroka, G., T. Miles, Y. Xu, J. Kohut, O. Schofield, and S. Glenn, 2016: Hurricane Irene sensitivity to stratified coastal ocean cooling. *Mon. Wea. Rev.*, **144**, 3507–3530, <https://doi.org/10.1175/MWR-D-15-0452.1>.
- Shay, L. K., and J. K. Brewster, 2010: Oceanic heat content variability in the eastern Pacific Ocean for hurricane intensity forecasting. *Mon. Wea. Rev.*, **138**, 2110–2131, <https://doi.org/10.1175/2010MWR3189.1>.
- , G. J. Goni, and P. G. Black, 2000: Effects of a warm oceanic feature on Hurricane Opal. *Mon. Wea. Rev.*, **128**, 1366–1383, [https://doi.org/10.1175/1520-0493\(2000\)128<1366:EOAWOF>2.0.CO;2](https://doi.org/10.1175/1520-0493(2000)128<1366:EOAWOF>2.0.CO;2).
- Shroyer, E., and Coauthors, 2021: Bay of Bengal intraseasonal oscillations and the 2018 monsoon onset. *Bull. Amer. Meteor. Soc.*, **102**, E1936–E1951, <https://doi.org/10.1175/BAMS-D-20-0113.1>.
- Stramma, L., P. Cornillon, and J. F. Price, 1986: Satellite observations of sea surface cooling by hurricanes. *J. Geophys. Res.*, **91**, 5031–5035, <https://doi.org/10.1029/JC091iC04p05031>.
- Wada, A., and N. Usui, 2007: Importance of tropical cyclone heat potential for tropical cyclone intensity and intensification in the western North Pacific. *J. Oceanogr.*, **63**, 427–447, <https://doi.org/10.1007/s10872-007-0039-0>.
- Walker, N. D., A. Haag, S. Balasubramanian, R. Leben, I. van Heerden, P. Kemp, and H. Mashriqui, 2006: Hurricane prediction: A century of advances. *Oceanography*, **19** (2), 24–36, <https://doi.org/10.5670/oceanog.2006.60>.
- Wood, K. R., and Coauthors, 2018: Results of the first Arctic Heat Open Science Experiment. *Bull. Amer. Meteor. Soc.*, **99**, 513–520, <https://doi.org/10.1175/BAMS-D-16-0323.1>.
- Yablonsky, R. M., and I. Ginis, 2009: Limitation of one-dimensional ocean models for coupled hurricane–ocean model forecasts. *Mon. Wea. Rev.*, **137**, 4410–4419, <https://doi.org/10.1175/2009MWR2863.1>.